Received: Added at production | Revised: Added at production | Accepted: Added at production

DOI: xxx/xxxx

RESEARCH ARTICLE

Three-Time-Scale Multi-Objective Optimal PID Control with Filter Design

Muhammad Aafaque*[1] | Almuatazbellah Boker[2] | Yousef Sardahi[3]

[1]R&D Center, Karl Dungs GmbH & Co. KG, D-73660 Urbach, Baden-Wuerttemberg, Germany
[2]Bradley Department of Electrical and Computer Engineering, Virginia Tech, Blacksburg, VA 24060, USA
[3]Department of Mechanical Engineering, Marshall University, Huntington, WV 25755, USA

Correspondence
*Muhammad Aafaque, R&D Center, Karl Dungs GmbH & Co. KG, D-73660 Urbach, Baden-Wuerttemberg, Germany.
Email: engr_aafaque@hotmail.com

Abstract

This paper presents the design of a multi-objective PID (proportional, integral, and derivative) controller in three-time scales for a system with load disturbances and sensor noise. The key to this design method is to divide the problem into three-time scales by following a singular perturbation approach, which allows for the optimization of fewer parameters in each time scale instead of all the three PID gains at once, hence less computation and design effort. The optimization objectives are the minimization of the overshoot and peak time, and the maximization of the closed-loop system's ability to reject noise and load disturbances. The impact of the integral action and filter on the optimal results is investigated by tuning the singular perturbation parameters. The obtained results show that the performance of the closed-loop system recovers the optimal solution, which is based on the fast subsystem, as the singular perturbation parameters get sufficiently small.

KEYWORDS:
Modified PID, Multi-objective optimization, Multi-time scale, Load disturbance, Measurement noise.

1 | INTRODUCTION

Feedback control design usually involves meeting multiple performance objectives which might be conflicting. It is sometimes not possible to simultaneously maximize and/or minimize the performance objectives. This paradox is especially clear when it comes to designing the parameters of the Proportional, Integral and Derivative (PID) controller. This is an important problem to solve as the PID controller is one of the popular feedback controllers that is widely used in the industry thanks to its simplicity and efficiency [24, 4].

Both the deterministic and stochastic frameworks have been proposed for the tuning of PID controllers [15]. The most commonly used conventional methods for tuning the PID controller are Trial and Error Method, Relay Tuning method, pole placement [34] and minimum variance techniques [35], Ziegler-Nichols step response method, Ziegler-Nichols frequency response method [36] and Cohen-Coon method (1953) [4]. The model of the system is not necessarily required to determine the gains of PID controller in such conventional methods which makes them advantageous over others [5]. However, such methods like Ziegler-Nichols may often lead to oscillations and big overshoot in the outputs when subjected to set-point changes as modeling uncertainties are involved despite good disturbance rejection [11]. Moreover, these methods are not intended to handle more than one design requirement in multi-objective settings and cannot deal with more than one cost function, for example, minimum rise time, overshoot, and regulation time at the same time, a new optimal design of the PID controller is required [31]. A number of attempts have been made to solve the tuning problem of gains of the PID controller, for example, in [20], an internal model control (IMC) based approach is used to tune the gains of the PID controller for the boost control system of the turbocharged engine using relay feedback experiment. In [18], a robust PI controller is designed for interval plants using worst-case gain and phase margin specifications in the presence of multiple crossover frequencies and the oblique wing aircraft is selected as an interval plant to demonstrate the results of the proposed

design. In [2], a technique is proposed for designing robust PID controller for a class of linear time-invariant single-input single-output systems using a linear programming approach for optimizing performance subject to robustness constraints, in which, the reference loop gain transfer function is shaped to form a convex region on the Nyquist diagram, where convex region is approximated by a set of lines to formulate the optimization problem.

Stochastic framework has gotten a lot of attention in solving the control problems [10], especially the multi-objective control problems [29]. Evolutionary algorithm (EA) is used in [16] to optimize the gains of PD controller for pneumatic rotary actuator servo system with friction compensation and the results are compared with that of differential evolution algorithm (DEA) and genetic algorithm (GA). Non-dominated sorting genetic algorithm (NSGA-II) is used for optimization of PID parameters for attitude stabilization of hovering quadcopter in [32], where a neural network algorithm, long short-term memory (LSTM), was used to evaluate the flight motions based on obtained PID parameters.

Feedback controllers come with a disadvantage of injecting measurement noise in the system which causes unwanted oscillations and, in consequence, wear and tear which may lead to possible breakdown [27]. As the measurement noise is usually dominated by higher frequencies [27], a low-pass filtering is required for the derivative part of the PID controller to limit the high-frequency gain [30]. The work in [26], proposed a second-order PID controller, which requires tuning of four parameters including the derivative filter factor and it was shown in that the derivative filter factor must be taken into account while optimizing the PID controller. This was a departure from the practice of designing commercial controllers as the filter gain is usually kept constant or totally ignored due to its noise amplification characteristics [28], especially when input disturbances are considered. The flip side is that this leads to a four-parameter design problem instead of three-parameter one, causing stability analysis more complex and tuning process more difficult or computationally demanding. However, using derivative filter factor in the PID controller improves the stability of closed-loop system, transient response and load disturbance rejection [28]. The results of [26] confirms this claim by following multi-objective optimization framework. Despite all this progress, improvement is still needed when it comes to design complexity and computational cost.

The desired output transient performances, and their insensitivity to plant parameter variations and unknown external disturbances, are ensured for full-order closed-loop nonlinear system by imposing sufficiently large mode separation rate between- fast and slow modes [19]. In [17], an anti-windup PI controller with a saturating integrator is proposed for a single-input single-output stable nonlinear system, and stability analysis is performed using a singular perturbation method by dividing the system into the slow and fast subsystem. However, this work does not consider measurement noise and neither filter is employed nor PI is tuned using any optimization techniques. In [33], the tracking problem for multiple-input-multiple-output (MIMO) nonlinear systems is addressed by multi-variable PI/PID controller based on time-scale separation (singular perturbation) technique, and author claims near perfect rejection of nonlinearities, unknown external disturbances and loop interactions due to increased degree of time-scale separation, but this work also does not take measurement noise into consideration and the parameters of the PI/PID controller are computed analytically instead of using any optimization technique.

In [21], a linear PID controller is used for tracking control of robotic manipulators actuated by compliant actuators and formulating the control problem into three-time-scale singular perturbation method where slow time-scale is included at the rigid dynamics, actual fast time-scale is included at the actuator dynamics and one virtual fast time-scale is included at controller dynamics. This approach not only provides semiglobal practical exponential stability using proper choice of control parameters, but also is structurally simple and model-free resulting in low implementation cost, and robust against external disturbances and parameter variations. Though this work utilizes the three-time scale technique to design PID controller, yet does not include the filter in the derivative part of the controller to counter the measurement noise.

This work proposes a method that designs the PID controller with a measurement derivative filter through solving a multi-objective optimization problem in a systematic and computationally efficient way. It avoids solving the optimization problem in one shot thus improving the result reported in [26], where four tuning parameters need to be optimized at the same time. The key idea in our work is to exploit the fact that the integrator dynamics are typically slower than the system dynamics while the filter dynamics are typically faster. This leads to modeling the closed-loop system in a three-time-scale fashion. Singular perturbation theory is then employed to decompose the closed-loop fourth-order system into three smaller-dimensional subsystems. This considerably simplifies the control design and allows for a targeted design thanks to the decoupling of the system states and parameters. Once the closed-loop system is decomposed into lower dimensional submodel, we design the gains of the PID controller using the non-dominated sorting genetic algorithm (NSGA-II), which is one of the most widely used multi-objective optimization algorithms [8], through minimizing the closed-loop response overshoot, peak time and maximizing the ability of the system to reject external load disturbances and measurement noises.

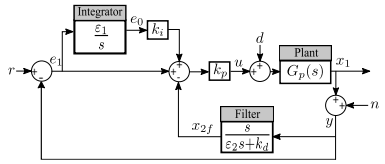

FIGURE 1 Diagram of the closed-loop system.

The main idea here is to account for the effect of the derivative filter on these conflicting design goals and present that to the decision-maker before the real implementation takes place. We show that the desired performance of the closed-loop system that is resulted from the decomposed system can be recovered after implementation by making the integrator sufficiently small and the filter sufficiently fast.

The reminder of this paper is organized as follows. Section 4 introduces the concept and the definition of the multi-objective optimization. The general formulation of the proposed control problem is proposed in Section 2. Section 5 introduces a numerical example, the multi-objective control design, and the results of the optimization process. Finally, the paper is concluded in Section 6.

2 | PROBLEM FORMULATION

Consider a plant G_P described by

$$\dot{x}_1 = x_2, \tag{1}$$

$$\dot{x}_2 = a_1 x_1 + a_2 x_2 + b\,(u + d)\,, \tag{2}$$

$$y = x_1 + n, \tag{3}$$

where $x = [x_1 \ x_2]^T \in \mathbb{R}^2$ is the vector of the system states, a_1, a_2 are systems parameters, $u \in \mathbb{R}$ is the control input and $b \neq 0$, $y \in \mathbb{R}$ is the measured output, d is the unknown external disturbance and n is a measurement (white) noise.

The objective of this work is to design a PID control law that allows the output to track a reference signal r while guaranteeing stability of the closed-loop system and achieving optimal transient performance. To deal with the effect of the noise, the derivative of the measured output is filtered through a low pass filter. The block diagram of the closed-loop system is shown in Figure 1. Accordingly, the objective is to design k_p, k_i, k_d, ε_1 and ε_2 so that y tracks a reference signal r.

Achieving an optimal transient performance requires solving a multi-objective optimization problem for the controller parameter. This means selecting the PID controller parameters plus the filter time constant to satisfy a number of objectives including minimizing the output overshoot, peak time, while minimizing the effect of disturbance and measurement noise. As it is well known, these objectives are in conflict with each other. This calls for employing a multi-objective optimization technique to select the four controller parameters for a four-dimensional system, which is comprised of the system dynamics (1)-(3) in addition to the integrator and filter dynamics.

3 | THREE TIME SCALES DESIGN

We will solve the control problem by employing the feedback control strategy shown in Figure 1. Key to this strategy is the use of the PID controller along with a filter to alleviate the effect of differentiating the noise. Following this approach, we will have five parameters to design; namely, $k_p, k_i, k_d, \varepsilon_1$ and ε_2. This problem has been solved in [26] with $\varepsilon_1 = 1$ using multi-objective optimization technique. In [26], the problem was solved in one shot by optimizing the controller parameters to achieve a number of conflicting objectives. Depending on the application and the plant, this approach might be computationally prohibitive, especially for large-scale systems. To overcome this limitation, we will solve this problem in a three-time-scale fashion by employing the singular perturbation technique [14] to design the control system. Accordingly, we propose the control law

$$u = k_p \left[\left(k_i e_0 + e_1 \right) - x_{2f} \right], \tag{4}$$

where $e_1 = r - y = r - x_1 - n$, and e_0 and x_{2f} are the states of integrator and filter , respectively, as indicated in Figure 1. We now augment the plant with the integrator and filter dynamics and write the closed-loop system as

$$\dot{e}_0 = \varepsilon_1 e_1, \tag{5}$$

$$\dot{x}_1 = x_2, \tag{6}$$

$$\dot{x}_2 = a_1 x_1 + a_2 x_2 + b \left[k_p \left(k_i e_0 + e_1 - x_{2f} \right) + d \right], \tag{7}$$

$$\varepsilon_2 \dot{x}_{2f} = -k_d x_{2f} + x_2 + \dot{n}. \tag{8}$$

Note that the upper script symbol dot denotes differentiation with respect to time scale t.

The time separation is done by first making sure the integrator is slow relative to the dynamics of the system. This implies making the rate of change of the integrator (the e_0 dynamics or equation (6)) to be smaller by at least an order of magnitude than that of the x dynamics or equations (7), (8). This means making the rate of change of (6) of the order $\mathcal{O}(\varepsilon_1)$, where $\varepsilon_1 < 1$, while the order of the rate of change of the dynamics of x is $\mathcal{O}(1)$. Second, we design the filter (equation (9)) to be faster than the system dynamics by an order of magnitude. This means making the rate of change of (6) of the order $\mathcal{O}(1/\varepsilon_2)$, where $\varepsilon_2 < 1$. Finally, to make sure that the time scale of the whole system is well defined and that the filter is faster than the integrator we choose $0 < \varepsilon_2 << \varepsilon_1 < 1$. Accordingly, the design procedure will be done in three time scales separately. First, we analyze the system in the slow time scale, denoted by θ and defined by $\theta = t\varepsilon_1$. As a result, the system dynamics in the θ time-scale can be written as

$$\frac{de_0}{d\theta} = e_1, \tag{9}$$

$$\varepsilon_1 \frac{dx_1}{d\theta} = x_2, \tag{10}$$

$$\varepsilon_1 \frac{dx_2}{d\theta} = a_1 x_1 + a_2 x_2 + b \left[k_p \left(k_i e_0 + e_1 - x_{2f} \right) + d \right], \tag{11}$$

$$\varepsilon_1\varepsilon_2\frac{dx_{2f}}{d\theta} = -k_d x_{2f} + x_2 + \varepsilon_1\frac{dn}{d\theta}. \tag{12}$$

To find the reduced (slow) subsystem, we let $\varepsilon_1 \to 0$ in (9)-(12). This leads to

$$x_2^s = 0, \quad x_{2f}^s = \frac{x_2^s}{k_d} = 0, \tag{13}$$

$$e_1^s = \frac{a_1 r - a_1 n + bk_p k_i e_0^s + bd}{\left(a_1 - bk_p\right)}, \tag{14}$$

which in turn leads to the reduced subsystem

$$\frac{de_0^s}{d\theta} = \frac{a_1 r - a_1 n + bk_p k_i e_0^s + bd}{\left(a_1 - bk_p\right)}, \quad e_0^s(0) = e_0(0). \tag{15}$$

Note that the superscript s used in (13)-(15) emphasizes the fact that these states belong to the slow time-scale. It should also be noted that (15) shows that the system in this time scale has scalar dynamics that depend on the noise and disturbance with k_p and k_i being the only design parameters.

We next analyze the system in the plant time scale t. In this case, we let $\varepsilon_1 \to 0$, which also implies $\varepsilon_2 \to 0$, in (5)-(8) so that we obtain

$$\dot{e}_0 = 0 \implies e_0 = e_0^s = \text{constant}, \tag{16}$$

$$x_{2f} = \frac{1}{k_d}(x_2 + \dot{n}). \tag{17}$$

Notice that due to the continuity of the system and as it is customary in singular perturbation analysis, we have (16) indicating that the slow integrator state is considered to be 'frozen' in this time-scale. Similarly, we regard e_1^s, x_1^s, x_2^s and x_{2f}^s as frozen in the t time scale, which means their derivative with respect to t is zero. In view of (17), we further have

$$\dot{x}_1 = x_2, \tag{18}$$

$$\begin{aligned}\dot{x}_2 = &\left(a_1 - bk_p\right)x_1 + \left(a_2 - \frac{bk_p}{k_d}\right)x_2 + bk_p k_i e_0^s \\ &+ bk_p r - bk_p n - \frac{bk_p}{k_d}\dot{n} + bd\end{aligned} \tag{19}$$

The term dependent on e_0^s in (19) is regarded as bias since e_0^s is a 'frozen' parameter in this time scale. Consequently, to remove this bias from (18)-(19), we employ

$$\begin{aligned}x_1^f =& x_1 + \frac{bk_p k_i e_0^s}{\left(a_1 - bk_p\right)}, \quad x_2^f = x_2 - x_2^s = x_2, \\ x_{2f}^f =& x_{2f} - x_{2f}^s = x_{2f},\end{aligned} \tag{20}$$

where the slow bias in x_2 and x_{2f} is zero as derived in (13). We now use (20) to get the t-time scale reduced system

$$\dot{x}_1^f = x_2^f, \quad x_1^f(0) = x_1(0) + \frac{bk_p k_i e_0^s}{\left(a_1 - bk_p\right)}e_0^s(0), \tag{21}$$

$$\begin{aligned}\dot{x}_2^f = &\left(a_1 - bk_p\right)x_1^f + \left(a_2 - \frac{bk_p}{k_d}\right)x_2^f + bk_p r \\ &- bk_p n - \frac{bk_p}{k_d}\dot{n} + bd, \quad x_2^f(0) = x_2(0),\end{aligned} \tag{22}$$

with

$$x_{2f}^f = \frac{1}{k_d}(x_2^f + \dot{n}). \tag{23}$$

Finally, we study the system in the fastest time scale, which we define as $\sigma = \frac{t}{\varepsilon_2}$. The closed-loop dynamics, in this case, will be:

$$\frac{de_0}{d\sigma} = \varepsilon_1\varepsilon_2 e_1, \tag{24}$$

$$\frac{dx_1}{d\sigma} = \varepsilon_2 x_2, \tag{25}$$

$$\frac{dx_2}{d\sigma} = \varepsilon_2\left[a_1 x_1 + a_2 x_2 + bk_p\left(k_i e_0 + e_1 - x_{2f}\right) + bd\right], \tag{26}$$

$$\frac{dx_{2f}}{d\sigma} = -k_d x_{2f} + x_2 + \frac{1}{\varepsilon_2}\frac{dn}{d\sigma}. \tag{27}$$

To find the fastest subsystem, we define

$$x_2^{ff} = x_{2f} - x_{2f}^f, \tag{28}$$

where x_{2f}^f is defined in (17). Note that, in view of $x_2 = x_2^f$ from (20) and in the σ time scale, (17) can be written as $x_{2f}^f = \frac{1}{k_p}(x_2 + \frac{1}{\varepsilon_2}\frac{dn}{d\sigma})$. Using this change of variables, substitute by (28) in (27). This eliminates ε_2 from (27). Now let $\varepsilon_2 \to 0$ in (24)-(27) so that we have

$$\frac{de_0}{d\sigma} = \frac{dx_1}{d\sigma} = \frac{dx_2}{d\sigma} = 0, \tag{29}$$

and

$$\frac{dx_{2f}^{ff}}{d\sigma} = -k_d x_{2f}^{ff}, \quad x_2^{ff}(0) = x_{2f}(0) - x_{2f}^f(0). \tag{30}$$

The decomposition of the three-time scale system is now summarized in the following proposition.

Proposition 1. In the limit as $\varepsilon_1 \to 0$ and $\varepsilon_2 \to 0$ and for all $0 < \varepsilon_2 << \varepsilon_1 < 1$ and for all $t \geq 0$, the closed-loop system (5)-(8) is decomposed into the following three subsystems:

1. the slow subsystem

$$\frac{de_0^s}{d\theta} = \frac{a_1 r - a_1 n + bk_p k_i e_0^s + bd}{\left(a_1 - bk_p\right)}, e_0^s(0) = e_0(0) \tag{31}$$

2. the fast subsystem

$$\begin{aligned}\dot{x}_1^f =& x_2^f, \\ \dot{x}_2^f =& \left(a_1 - bk_p\right)x_1^f + \left(a_2 - \frac{bk_p}{k_d}\right)x_2^f + bk_p r \\ &- bk_p n - \frac{bk_p}{k_d}\dot{n} + bd, \\ x_1^f(0) = x_1(0) + &\frac{bk_p k_i e_0^s}{\left(a_1 - bk_p\right)}e_0^s(0), \quad x_2^f(0) = x_2(0),\end{aligned} \tag{32}$$

3. the fastest subsystem

$$\frac{dx_{2f}^{ff}}{d\sigma} = -k_d x_{2f}^{ff}, x_2^{ff}(0) = x_{2f}(0) - x_{2f}^f(0) \tag{33}$$

Remark 1. Singular perturbation theory [14] suggests that the responses of the reduced subsystems (31)-(33) become close to the response of the closed-loop system (5)-(8) as ε_2 and ε_1 become sufficiently small. This is shown in the case of $\varepsilon_2 = 1$ and the measurement noise n and its derivative are both zero-mean stationary white noise [Theorem 2.1, Ch. 4 [14]]. In this case, the closed-loop system exhibits a two time-scale structure. This result further implies that if the parameters k_p, k_d, k_i

are chosen such that the reduced subsystems are asymptotically stable then there exists an ε_1^* such that for all $\varepsilon_1 \in (0, \varepsilon_1^*)$ and for all $t \geq 0$ the error between the original states of the system (5)-(8) and the states of the reduced subsystems to be $O(\varepsilon_1^{1/2})$. This means that as ε_1 gets smaller the performance of the reduced subsystems gets close to the original one.

Remark 2. It is clear from Proposition 1 that the closed-loop system (5)-(8) is decomposed into three lower dimensional and decoupled systems. This allows for the design of the the controller parameters in the following way:

1. Consider subsystem (32) and design k_p and k_d by solving a multi-objective optimization problem to optimize a number of conflicting objectives including the minimization of the effect of noise and disturbance. The choice of k_p and k_d needs to be constrained to guarantee stability of (32). In addition, k_d needs to be chosen to be positive to guarantee stability of (33).
2. Step 1 results in optimal values for k_d and k_p. We then use the values obtained for k_p to design k_i so to guarantee stability of (31).
3. Choose $[\varepsilon_1, \varepsilon_2]$ small enough for acceptable performance.

This procedure is illustrated by a simulation example in Section 5.

Remark 3. It is important to note that the change of variables (20) does not depend on the disturbance nor noise. This allows for design and analysis to be performed on the reduced system (32) and then similar performance is expected for the original system for sufficiently small ε_1. This is different than the change of variables suggested by [14] to analyze the two-time-scale PID controller in the absence of measurement noise and filter. In that case, the objective was to show that the disturbance effect can be decoupled in different time scales.

4 | MULTI-OBJECTIVE OPTIMIZATION

4.1 | Basic Concept

Multi-objective optimization is an area of multiple criteria decision-making. It deals with mathematical optimization problems involving two or more conflicting fitness functions to be optimized at the same time. Multi-objective optimization problems (MOPs) have gained a lot of attention recently because of their enormous applications in engineering, economics and logistics, just to name a few. In mathematical terms, a MOP can be stated as follows:

$$\min_{\mathbf{k} \in Q} \{\mathbf{F}(\mathbf{k})\}, \tag{34}$$

where $\mathbf{F} : Q \to \mathbf{R}^k$, $\mathbf{F}(\mathbf{k}) = [f_1(\mathbf{k}), \dots, f_k(\mathbf{k})]$ is the map that consists of the objective functions $f_i : Q \to R^1$ under consideration, and $\mathbf{k} \in Q$ is a q-dimensional vector of design parameters. The domain $Q \subset \mathbf{R}^q$ can in general be expressed by inequality and equality constraints:

$$\begin{aligned} Q = \{\mathbf{k} \in \mathbf{R}^q \mid g_i(\mathbf{k}) \leq 0,\ i = 1, \dots, l, \\ \text{and } h_j(\mathbf{k}) = 0,\ j = 1, \dots, m\}. \end{aligned} \tag{35}$$

The solution of MOPs comprises a set known as the *Pareto set* and the corresponding set of objective values called *Pareto front*. The optimal solution is obtained using the *dominancy* concept [22]. For a comprehensive survey of the methods used to solve the MOPs problems, the reader can consult [23, 1, 25]. In this paper, the non-dominated sorting genetic algorithm (NSGA-II) is used to solve the MOP at hand. NSGA-II is the improved version of NSGA, which is faster, has a better sorting algorithm, includes an elitism mechanism, and eliminates the need for the sharing parameter that was introduced in NSGA [8]. We next provide more details about the algorithm.

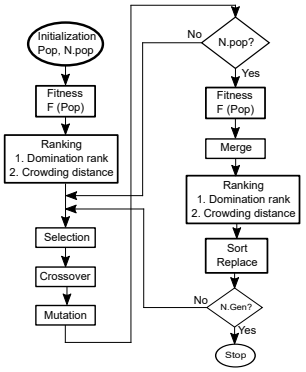

FIGURE 2 Flow chart of NSGA-II

4.2 | NSGA-II

The NSGA-II algorithm consists of eight basic operations: Initialization, fitness evaluation, domination ranking, crowding distance calculation, selection, crossover, mutation, and combination to solve MOPs [8] as depicted in Figure (2). The initialization algorithm is executed first to generate a random population matrix, **Pop**, within the specified lower and upper bounds of the tuning parameters. This matrix is passed to the the fitness algorithm, **F**(**Pop**), to compute the cost functions at each candidate solution. Then, the ranking algorithm is called to place the candidate solutions at different fronts based on their non-domination ranks and crowding distance values. That is, the solutions in the first front dominate all the other solutions, while the solutions in the second front are dominated only by the members in the first front, and so on. To ensure a diverse and distributed solution, the crowding distance is calculated for each solution front-wise. The crowding distance measures how far a solution is from its neighboring solutions within the same front. Larger crowding distance values indicate a better distribution of the solutions. After ranking, the selection algorithm is called to randomly select parents that

will be used to produce the next generation of candidate solutions. To this end, the binary tournament selection algorithm is usually used. The selection process starts with generating two uniformly distributed random integer numbers between 1 and $N.pop$ (number of candidate solutions). The two numbers are used to select two candidate parents from **Pop**. The parent with either a smaller rank or bigger crowding distance than the other is chosen. The selection process continues for $N.pop$ times. After that, the crossover process such as the arithmetic crossover algorithm [3, 7] and a mutation algorithm such as the simple mutation approach [13] are executed using the selected parents to produce childern. These two operations are executed $N.pop/2$ times producing a new offspring of size $N.pop$. After that, the children are merged with the current population. This combination guarantees the elitism of the best individuals. Finally, the merged population is sorted based on crowding distance and rank values. The new generation is produced from the sorted population until the number of population reaches $N.pop$. The selection, crossover, mutation, merging, ranking, and sorting process is repeated over and over until the number of generations reaches a preselected $N.Gen$.

4.3 | Multi-objective Optimal Control

The closed-loop system should be designed such that the effect of $D(s)$ and $N(s)$ on the output is minimal. Here, $D(s)$ and $N(s)$ are the Laplace transforms of $n(t)$ and $d(t)$, respectively, shown in Figure 1. However, these two objectives are conflicting and can not be made minimum at the same time. Instead, optimal trade-off solutions between them can be found. Another example of conflicting design goals is the problem of maximizing the controlled system speed of response (by minimizing the peak time t_p) and minimizing the overshoot (M_p). Thus, a MOP should be formulated to handle these conflicting design objectives. To account for the impact of $N(s)$ and $D(s)$ on the performance of the closed-loop system and numerically compute t_p and M_p, we define with the help of Figure 1 three functions: the complementary sensitivity transfer function $CSTF$, the load disturbance sensitivity transfer function $LDSTF$, and the noise sensitivity transfer function $NSTF$ as follows:

$$CSTF(s) = \frac{C(s)G_p(s)}{1 + C(s)G_p(s)F(s)}, \tag{36}$$

$$LDSTF(s) = \frac{G_p(s)}{1 + C(s)G_p(s)F(s)}, \tag{37}$$

$$NSTF(s) = \frac{C(s)G_p(s)F(s)}{1 + C(s)G_p(s)F(s)}, \tag{38}$$

where $C(s) = k_p\left(1 + \varepsilon_1 \frac{k_i}{s}\right)$, $G_p(s) = \frac{b}{s^2 - a_2 s - a_1}$ and $F(s) = 1 + \left(\frac{s}{\varepsilon_2 s + k_d}\right)\left(\frac{s}{s + \varepsilon_1 k_i}\right)$.

The transfer functions (36)-(38) are used for the controller design in the following manner; First, the step response of (36) is simulated and used to compute t_p and M_p, which can then be minimized. Similarly, the frequency responses of (38) and (37) are generated and used to minimize the impact of $N(s)$ and $D(s)$ on the closed-loop control system. This procedure is illustrated further in the Section 5.

Our strategy is to use the three lower dimensional subsystems (31)-(33) to solve the multi-objective design problem and then we select ε_1 and ε_2 small enough to recover the desired performance. Towards this goal, we note that the fast subsystem has only two design parameters (k_p and k_d), which is very attractive from the optimization perspective since it leads to less computation load. Using this subsystem, the complementary sensitivity transfer function $CSTF^f$, the load disturbance sensitivity transfer function $LDSTF^f$, and the noise sensitivity transfer function $NSTF^f$ of the fast subsystem read

$$CSTF^f(s) = \frac{X_1^f(s)}{R(s)} = -\frac{bk_p}{s^2 - \left(a_2 - \frac{bk_p}{k_d}\right)s - \left(a_1 - bk_p\right)} \tag{39}$$

$$LDSTF^f(s) = \frac{X_1^f(s)}{D(s)} = \frac{b}{s^2 - \left(a_2 - \frac{bk_p}{k_d}\right)s - \left(a_1 - bk_p\right)} \tag{40}$$

$$NSTF^f(s) = \frac{X_1^f(s)}{N(s)} = -\frac{bk_p\left(1 + \frac{s}{k_d}\right)}{s^2 - \left(a_2 - \frac{bk_p}{k_d}\right)s - \left(a_1 - bk_p\right)} \tag{41}$$

It is worth noting that the three functions (39)-(41) can also be obtained from Figure 1 by setting $\varepsilon_1 = \varepsilon_2 = 0$ and simplifying the block diagram. The functions (39)-(41) can now be used to solve the multi-objective optimization problem.

5 | SIMULATION EXAMPLE: DC SERVO MOTOR

5.1 | System Models

Consider a DC servo motor system represented by the equations

$$\dot{x}_1 = x_2, \tag{42}$$

$$\dot{x}_2 = \frac{-1}{\tau}x_2 + \frac{K}{\tau}(u + d), \tag{43}$$

$$y = x_1 + n, \tag{44}$$

where $x = [x_1\ x_2]^T$ is the vector of the system states, u is the control input, y is the measured output, n is measurement noise and d is the unknown external disturbances, i.e. unknown load torque. It is assumed that d and its derivatives are bounded.

The control law defined in (4) will be used to track the reference signal r. The parameters K_p, K_i, K_d, ε_1 and ε_2 will be designed according to the procedure defined in Remark 2 in Sections 3 and following the multi-objective optimization approach described in Section 4.

By comparing the DC motor model in (42)-(44) with the generic model in (1) - (3), we have the following correspondence; $a_1 = 0$, $a_2 = -\frac{1}{\tau}$, $b = \frac{K}{\tau}$. Using these values and in

view of the singular perturbation decomposition (31)-(33), the slow subsystem is given by

$$\frac{de_0^s}{d\theta} = -k_i e_0^s - \frac{1}{k_p} d, \tag{45}$$

where $e_0^s(0) = e_0(0)$. Likewise, the fast subsystem reads

$$\dot{x}_1^f = x_2^f, \tag{46}$$

$$\begin{aligned} \dot{x}_2^f = &-\frac{K}{\tau} k_p x_1^f - \frac{1}{\tau}\left(1 + \frac{k_p}{k_d}\right) x_2^f - \frac{K}{\tau} k_p n + \frac{K}{\tau} d \\ &- \frac{K}{\tau}\frac{k_p}{k_d}\dot{n} + \frac{K}{\tau} k_p r. \end{aligned} \tag{47}$$

$$x_1^f(0) = x_1(0) - k_i e_0^s(0), \quad x_2^f(0) = x_2(0)$$

Finally, the fastest subsystem is provided by

$$\frac{dx_{2f}^{ff}}{d\sigma} = -k_d x_{2f}^{ff}. \tag{48}$$

After obtaining the optimal solutions for k_p and k_d, we will use them to design the remaining parameters by using the slow (45) and the fastest subsystems (48). This will be explained further in the next subsection.

5.2 | Multi-Objective Optimal Control Design

Consider a multi-objective control design for the fast subsystem (46)-(47), where the gain $\mathbf{k} = [k_p, k_d]$ are the design parameters. The chosen design space for the parameters is as follows,

$$Q = \{\mathbf{k} \in [1, 60] \times [49, 240] \subset \mathbf{R}^2\}. \tag{49}$$

The values of k_p and k_d are chosen such the stability of (46)-(47) is guaranteed. In addition, k_d is chosen to be positive to guarantee stability of (48). The upper boundaries are arbitrarily chosen. These constraints on the parameter space are used during the simultaneous minimization of the following design objectives,

$$\min_{\mathbf{k}\in Q}\{t_p, M_p, \left\|LDSTF^f(j\omega)\right\|_\infty, \left\|NSTF^f(j\omega)\right\|_\infty\}, \tag{50}$$

where t_p is the peak time, M_p is the maximum percentage overshoot, $\left\|LDSTF^f(j\omega)\right\|_\infty$ and $\left\|NSTF^f(j\omega)\right\|_\infty$ are the load disturbance and noise rejection capabilities of the closed-loop system, respectively. The terms $\left\|LDSTF^f(j\omega)\right\|_\infty$ and $\left\|NSTF^f(j\omega)\right\|_\infty$ are given by

$$\left\|LDSTF^f(j\omega)\right\|_\infty = \sup_{\omega<\omega_c} \sigma(LDSTF^f(j\omega)), \tag{51}$$

$$\left\|NSTF^f(j\omega)\right\|_\infty = \sup_{\omega>\omega_c} \sigma(NSTF^f(j\omega)), \tag{52}$$

where σ and ω_c are the largest singular value and the threshold frequency of the transfer function, respectively. Typically, measurement noises are most influential at high frequencies and load disturbances are most influential at low frequencies. Accordingly, for this application we use ω_c to be at 1 rad/s. A controlled system is considered to have good load disturbance and noise rejection capabilities if it conforms to $\left\|LDSTF^f(j\omega)\right\|_\infty << 1$, and $\left\|NSTF^f(j\omega)\right\|_\infty << 1$, respectively. Therefore, the constraints $\left\|LDSTF^f(j\omega)\right\|_\infty < 1$, and $\left\|NSTF^f(j\omega)\right\|_\infty < 1$ are also imposed to ensure these capabilities.

The non-dominated sorting genetic algorithm (NSGA-II) is utilized to solve this multi-optimization problem. The reader can consult [6] for in-depth understanding about this algorithm. According to Matlab documentation, the population size can be configured in multiple ways and by default, population size is 15 times the number of the design variables *nvars*. And, the maximum number of generations should not exceed 200 × *nvars*. In this study, the population size and number of generation are set to 200.

The Matlab version of the NSGA-II is used to solve the MOP defined in (50) by tuning the parameters defined in (49). According to the literature, NSAG-II performs well on two-objective and three-objective problems. For more than three objectives, a large number of populations should be used to enhance the searchability of the algorithm [12]. Also, the algorithm converges to the true Pareto front if the number of design parameters is less than or equal to 128 [9]. In this paper, the size of the objective space is 4 and that of decision variable space is 2. The population size and number of generation are set to 200. Therefore, NSGA-II is expected to perform well at solving the optimization problem at hand.

5.3 | Simulation Results

The Pareto fronts from the fast subsystem, and the impact of ε_1 and ε_2 on the optimal solution and closed-loop system response at different solutions are discussed here. In the simulation results, we use $\varepsilon_1 = 10\varepsilon_2$. However, other choices, such that ε_2 is sufficiently smaller than ε_1, will show a similar trend.

Two projections from the 4-D Pareto front are shown in Figure 3(a) and Figure 3(b). Figure 3(a) shows the conflicting relationship between the overshoot M_p and peak time t_p, while Figure 3(b) shows the conflict between the objective of minimizing the impact of measurement noise and load disturbance. The figures also show how ε_1 and ε_2 affect the optimal solution. For example, the lower optimal values of M_p increase as ε_1 and ε_2 increase. On the other side, the upper values of t_p decrease as ε_1 and ε_2 go up. So, a control system designer should expect smaller t_p but larger overshoot for every point on the front after adding the integral action and filter to the closed-loop response. On the other hand, Figure 3(b) shows that the optimal solutions from the fast subsystem represent the maximum values of $\left\|LDSTF^f(j\omega)\right\|_\infty$ and $\left\|NSTF^f(j\omega)\right\|_\infty$. That is, implementing the integral control and filter will lead to smaller values of these design objectives, and in turn better rejection of external noise and disturbance.

Three points of interest are labeled in Figure 3(a) and Figure 3(b). P_I has the coordinate of the minimum objective

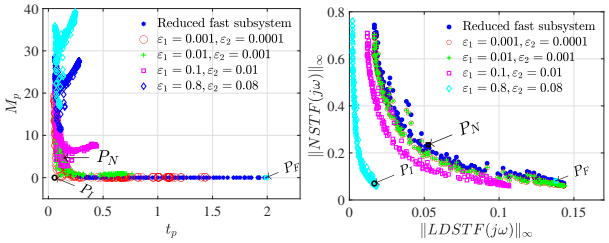

(a) (b)

FIGURE 3 (a) M_p vs. t_p for different values of ε_1 and ε_2, (b) $\|NSTF^j(j\omega)\|_\infty$ vs. $\|LDSF^j(j\omega)\|_\infty$ for different values of ε_1 and ε_2. Here P_I is the ideal solution, P_N is the knee-point and P_F is the far-point.

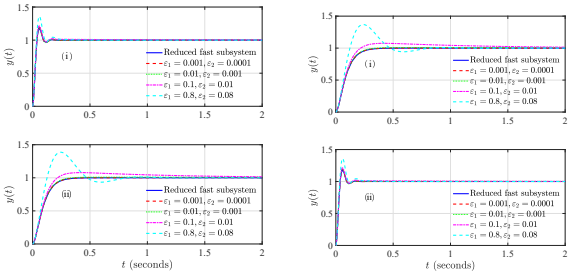

(a) (b)

FIGURE 4 (a) Closed-loop system response at: (i) min(t_p) with $k_p = 59.9394$, $k_d = 238.2716$, and (ii) max(t_p) with $k_p = 7.2439$ and $k_d = 129.2492$, (b) Closed-loop system response at: (i) min(M_p) with $k_p = 8.1148$, $k_d = 68.8419$, and (ii) max(M_p) with $k_p = 29.9168$, $k_d = 238.7562$.

functions, and is thus an ideal point not on the Pareto front. P_N, knee point, is a point on the Pareto front and the closest to P_I . This point can be more attractive to the designer than other optimal options since it is the closet to the ideal solution. P_F is a point on the Pareto front that has the largest Euclidean distance from P_I . Even though P_F is one of the optimal solutions, it could be less attractive to the decision-maker because it is far away from the ideal solution. These points illustrate the properties of the multi-objective optimization design.

Furthermore, we notice that the results agree with the singular perturbation theory [14] that suggests that the responses of the reduced subsystems (46)-(47) become close to the response of the closed-loop system (42)-(43) as ε_2 and ε_1 become sufficiently small. That is, the solution of the optimization problem (50) using the fast-subsystem (46)-(47) becomes closer to that of the closed-loop system (42)-(43) as the singular perturbation parameters approach zero.

Figure 4(a) shows the closed-loop response when t_p from the Pareto front is the largest (Figure 4(a)(i)) and when it is the smallest (Figure 4(a)(ii)). It is evident that fast system responses are associated with large overshoot values while those at $max(t_p)$ are associated with smaller overshoot values. These observations agree with the results depicted in

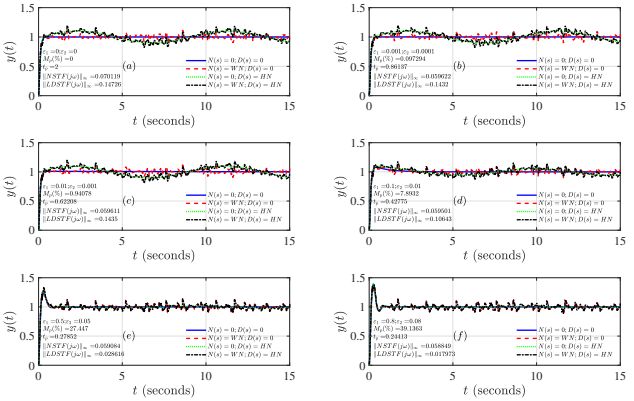

FIGURE 5 Closed-loop system response at min($\|NSTF^j(j\omega)\|_\infty$) with $k_p = 6.9854$, $k_d = 236.6588$ and $k_i = 10$ (a) with $\varepsilon_1 = 0, \varepsilon_2 = 0$; (b) with $\varepsilon_1 = 0.001$, $\varepsilon_2 = 0.0001$; (c) with $\varepsilon_1 = 0.01$, $\varepsilon_2 = 0.001$; (d) with $\varepsilon_1 = 0.1$, $\varepsilon_2 = 0.01$; (e) with $\varepsilon_1 = 0.5$, $\varepsilon_2 = 0.05$; and (f) with $\varepsilon_1 = 0.8$, $\varepsilon_2 = 0.08$.

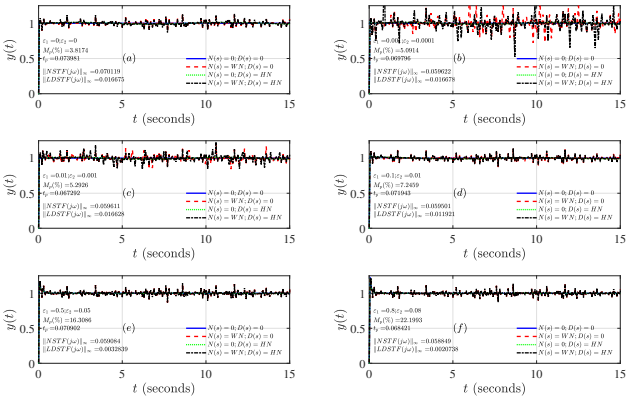

FIGURE 6 Closed-loop system response at min($\|LDSF^j(j\omega)\|_\infty$) with $k_p = 59.9720$, $k_d = 92.4594$ and $k_i = 10$ (a) with $\varepsilon_1 = 0, \varepsilon_2 = 0$; (b) with $\varepsilon_1 = 0.001$, $\varepsilon_2 = 0.0001$; (c) with $\varepsilon_1 = 0.01$, $\varepsilon_2 = 0.001$; (d) with $\varepsilon_1 = 0.1$, $\varepsilon_2 = 0.01$; (e) with $\varepsilon_1 = 0.5$, $\varepsilon_2 = 0.05$; and (f) with $\varepsilon_1 = 0.8$, $\varepsilon_2 = 0.08$;

Figure 3(a). Also, we notice that the overshoot goes up and peak time goes down as we increase the values of ε_1 and ε_2.

Figure 4(b) shows the controlled system response at the maximum and minimum values of M_p. Since there is a conflict relationship between M_p and t_p, we notice that the closed-loop behavior at $min(M_p)$ (Figure 4(b)(i)) is exactly the same as that when t_p is the largest (Figure 4(a)(ii)) and vice versa.

Figure 5 shows the closed-loop response at min($\|NSTF^j(j\omega)\|_\infty$) with $k_p = 6.9854$, $k_d = 236.6588$ and $k_i = 10$ for different values of ε_1 and ε_2. Here, the noise signal is assumed to be a white noise with variance 0.0001 and zero mean. As evident from (Figure 5(a)), the response at $min(\|NSTF^j(j\omega)\|_\infty)$ is associated with an increase in the percentage overshoot M_p but smaller t_p and better rejection of noise and disturbance as the singular perturbation parameters get large. Figure 6, on the other hand, shows the closed-loop response for min($\|LDSF^j(j\omega)\|_\infty$) with $k_p = 59.9720$,

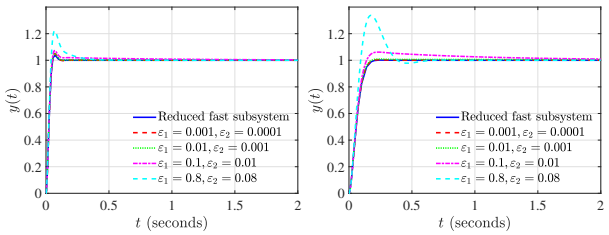

(a) (b)

FIGURE 7 (a) Closed-loop system response at P_N with $k_p = 59.9720$ and $k_d = 92.4594$, (b) Closed-loop system response at P_F with $k_p = 12.2549$ and $k_d = 102.2563$.

$k_d = 92.4594$ and $k_i = 10$. In this case, the load disturbance is modelled by a harmonic signal, $d(s) = 0.7 \times sin(0.7t)$ represented by HN in figures. As the singular perturbation parameters get large, we notice better disturbance rejection, but at the expense of M_p. On other side, t_p gets smaller which indicates faster response. This is expected since larger ϵ_1 indicates larger integration action, which is known to make the overshoot goes up. As a result, the peak time goes down.

Figure 7(a) shows the closed-loop response at P_N while Figure 7(b) depicts the controlled system response at P_F. In both figures, we notice that the closed-loop response shows faster response and larger overshoot as ϵ_1 and ϵ_2 increase. However, the optimal solution at P_N shows less increase in M_p as the integral and filter terms enter the system.

Moreover, it should be pointed out that the proposed three-time scale design reduces the computation time significantly. On Core-i7 PC with four cores, eight logical processors, and 1.99 GHz base speed, the solution of the MOP under three-time scale separation takes about 2 minutes, while it increases to 34 minutes when all design parameters (k_p, k_d, k_i, and ϵ_2) are considered at the same time, as reported in [26].

6 | CONCLUSION

We have studied the multi-objective optimal design of the PID controller in three time scales for a system having a load disturbance and corrupted feedback signal. An optimization problem with four design objectives and two design parameters is solved by the NSGA-II algorithm. The results show that the optimal solutions obtained by using the reduced fast subsystem lead to better rejection of noise and load disturbance, and faster closed-loop response, but higher overshoot values than those on the front after adding the integral action and filter. Also, the results show that the Pareto front of the closed-loop system gets closer to that of the reduced subsystem as the singular perturbation parameters become sufficiently small. For future work, it is interesting to investigate how the proposed scheme extends to the case of nonlinear systems and systems with more than second-order dynamics.

References

[1] Z. N. Ansari and S. D. Daxini, *A state-of-the-art review on meta-heuristics application in remanufacturing*, Archives of Computational Methods in Engineering (2021), 1–44.

[2] C. P. B. Barros, P. R. Barros, and J. S. da Rocha Neto, *Loop shaping for pid controller design based on time and frequency specifications*, IFAC-PapersOnLine **51** (2018), no. 4, 592–597.

[3] H.-G. Beyer and K. Deb, *On self-adaptive features in real-parameter evolutionary algorithms*, IEEE Transactions on evolutionary computation **5** (2001), no. 3, 250–270.

[4] R. P. Borase et al., *A review of PID control, tuning methods and applications*, International Journal of Dynamics and Control **9** (2021), no. 2, 818–827.

[5] Š. Bucz and A. Kozáková, *Advanced methods of PID controller tuning for specified performance*, PID Control for Industrial Processes (2018), 73–119.

[6] K. Deb, *Multi-Objective Optimization Using Evolutionary Algorithms*, Wiley, New York, 2001.

[7] K. Deb, R. B. Agrawal et al., *Simulated binary crossover for continuous search space*, Complex systems **9** (1995), no. 2, 115–148.

[8] K. Deb et al., *A fast and elitist multiobjective genetic algorithm: NSGA-II*, IEEE transactions on evolutionary computation **6** (2002), no. 2, 182–197.

[9] J. J. Durillo et al., *A study of multiobjective metaheuristics when solving parameter scalable problems*, IEEE Transactions on Evolutionary Computation **14** (2010), no. 4, 618–635.

[10] Y. Feng, X. Chen, and G. Gu, *Multiobjective H_2 / H_∞ control design subject to multiplicative input dependent noises*, SIAM Journal on Control and Optimization **56** (2018), no. 1, 253–271.

[11] M. Huba et al., *Making the PI and PID controller tuning inspired by ziegler and nichols precise and reliable*, Sensors **21** (2021), no. 18, 6157.

[12] H. Ishibuchi et al., *Evolutionary many-objective optimization by NSGA-II and MOEA/D with large populations*, *2009 IEEE International Conference on Systems, Man and Cybernetics*, IEEE, 1758–1763.

[13] M. R. O. Kakde, *Survey on multiobjective evolutionary and real coded genetic algorithms*, *Proceedings of the 8th Asia Pacific symposium on intelligent and evolutionary systems*, Citeseer, 150–161.

[14] P. Kokotović, H. K. Khalil, and J. O'reilly, *Singular perturbation methods in control: analysis and design*, SIAM, 1999.

[15] N. P. Lawrence et al., *Deep reinforcement learning with shallow controllers: An experimental application to PID tuning*, Control Engineering Practice **121** (2022), 105046.

[16] K. Li et al., *Evolutionary algorithm-based friction feedforward compensation for a pneumatic rotary actuator servo system*, Applied Sciences **8** (2018), no. 9, 1623.

[17] P. Lorenzetti and G. Weiss, *Saturating pi control of stable nonlinear systems using singular perturbations*, IEEE Transactions on Automatic Control (2022).

[18] R. Matušů et al., *Design of robust PI controllers for interval plants with worst-case gain and phase margin specifications in presence of multiple crossover frequencies*, IEEE Access **10** (2022), 67713–67726.

[19] Y. Mchaouar et al., *Nonlinear control of single-phase shunt active power filters with theoretical analysis via singular perturbation*, *2018 5th International Conference on Electrical and Electronic Engineering (ICEEE)*, IEEE, 67–72.

[20] H. R. Ossareh et al., *An internal model control-based approach for characterization and controller tuning of turbocharged gasoline engines*, IEEE Transactions on Control Systems Technology **29** (2019), no. 2, 866–875.

[21] Y. Pan, X. Li, and H. Yu, *Efficient PID tracking control of robotic manipulators driven by compliant actuators*, IEEE Transactions on Control Systems Technology **27** (2018), no. 2, 915–922.

[22] V. Pareto, *Manual of Political Economy*, The MacMillan Press, London, 1971 (original edition in French in 1927).

[23] Z.-C. Qin, Y. Xin, and J.-Q. Sun, *Multi-objective optimal motion control of a laboratory helicopter based on parallel simple cell mapping method*, Asian Journal of Control **22** (2020), no. 4, 1565–1578.

[24] N. H. Sahrir and M. A. Mohd Basri, *Modelling and manual tuning PID control of quadcopter*, *Control, Instrumentation and Mechatronics: Theory and Practice*, Springer, 2022. 346–357.

[25] N. Saini and S. Saha, *Multi-objective optimization techniques: A survey of the state-of-the-art and applications*, The European Physical Journal Special Topics **230** (2021), no. 10, 2319–2335.

[26] Y. Sardahi and A. Boker, *Multi-objective optimal design of four-parameter pid controls*, *Dynamic Systems and Control Conference*, vol. 51890, American Society of Mechanical Engineers, V001T01A001.

[27] V. R. Segovia, T. Hägglund, and K. J. Åström, *Measurement noise filtering for PID controllers*, Journal of Process Control **24** (2014), no. 4, 299–313.

[28] M. A. Siddiqui, M. N. Anwar, and S. H. Laskar, *Tuning of PIDF controller in parallel control structure for integrating process with time delay and inverse response characteristic*, Journal of Control, Automation and Electrical Systems **31** (2020), no. 4, 829–841.

[29] S. Sui, C. P. Chen, and S. Tong, *Fuzzy adaptive finite-time control design for nontriangular stochastic nonlinear systems*, IEEE Transactions on Fuzzy Systems **27** (2018), no. 1, 172–184.

[30] I. Tejado et al., *Back to basics: Meaning of the parameters of fractional order PID controllers*, Mathematics **7** (2019), no. 6, 530.

[31] B. Verma and P. K. Padhy, *Robust fine tuning of optimal PID controller with guaranteed robustness*, IEEE Transactions on Industrial Electronics **67** (2019), no. 6, 4911–4920.

[32] J. Yoon and J. Doh, *Optimal PID control for hovering stabilization of quadcopter using long short term memory*, Advanced Engineering Informatics **53** (2022), 101679.

[33] V. D. Yurkevich, *MIMO tracking PI/PID controller design for nonlinear systems based on singular perturbation technique*, IFAC-PapersOnLine **48** (2015), no. 11, 760–765.

[34] W. Zhang, Y. Cui, and X. Ding, *An improved analytical tuning rule of a robust PID controller for integrating systems with time delay based on the multiple dominant pole-placement method*, Symmetry **12** (2020), no. 9, 1449.

[35] N. Zhu, X.-T. Gao, and C.-Q. Huang, *A data-driven approach for on-line auto-tuning of minimum variance PID controller*, ISA transactions (2022).

[36] J. G. Ziegler, N. B. Nichols et al., *Optimum settings for automatic controllers*, trans. ASME **64** (1942), no. 11.

Muhammad Aafaque is an Embedded Software Engineer at the R & D center of Karl DUNGS GmbH & Co. KG., Urbach, Germany, where since 2017 he is involved in research and development of state-of-the-art industrial and commercial combustion control systems. He received his B.Eng in Industrial Electronics from N.E.D. University of Engineering Technology, Karachi, Pakistan in 2009, M.S. in Control Systems Engineering from National University of Sciences and Technology (NUST), Islamabad, Pakistan in 2014 and M.Sc. in Communications Engineering from Technical University of Munich (TUM), Munich, Germany in 2017. Mr. Aafaque had been involved in research and development of attitude and orbital control subsystem (AOCS) of low-earth orbit satellite at Pakistan's space agency SUPARCO during 2011-2015. His research interests include linear and nonlinear control systems, embedded systems and networked control systems.

Dr. Almuatazbellah M. Boker is a Collegiate Assistant Professor at the Bradley Department of Electrical and Computer Engineering, Virginia Tech. He received his B.Eng in Mechatronics Engineering from the University of Leeds, UK, in 2002, his M.S. in Control Systems Engineering from the University of Sheffield, UK, in 2003 and his Ph.D. in Electrical Engineering from Michigan State University in 2013. Dr. Boker worked as an Assistant Lecturer at the Electrical and Electronics Engineering Department, University of Benghazi, Libya, 2004-2008, and as a Post Doctoral Research Scholar at the NSF FREEDM Center, part of the Electrical and Computer Engineering Department, North Carolina State University, 2014-2015 and as an Assistant Professor at the Computer Sciences and Electrical Engineering Department, Marshall University, 2016-2019. Dr. Boker is an expert on the analysis and control of nonlinear systems. His research interests include data-driven estimation and control of dynamic systems. Dr. Boker is an Associate Editor of the IEEE Control Systems Society Conference Editorial Board. He received the 2002 Smallpeice Trust Prize from the University of Leeds for "an outstanding work on mechatronics", and the best poster award, 2012, Graduate Research Symposium, Michigan State University.

Dr. Yousef Sardahi is an assistant professor in the Weisberg Department of Mechanical Engineering at Marshall University. He earned Ph.D. from the Department of Mechanical Engineering at the University of California, Merced in 2016. His research interest includes Control System Design and Multi-Objective Optimization. His teaching experience includes Control Systems, Digital Controls, Automation and Control, System Modeling, Advanced Vibrations, Mechatronics, Circuits and Instrumentations, and Mechanical Engineering Computations.

□